



ELSEVIER

Available online at www.sciencedirect.com

SCIENCE @ DIRECT®

Journal of Crystal Growth 275 (2005) 624–638

JOURNAL OF **CRYSTAL
GROWTH**

www.elsevier.com/locate/jcrysgro

Transient growth and interaction of equiaxed dendrites

I. Steinbach^a, H.-J. Diepers^a, C. Beckermann^{b,*}

^aACCESS e.V., RWTH-Aachen, Intzestr. 5, 52072 Aachen, Germany

^bDepartment of Mechanical and Industrial Engineering, The University of Iowa, 2412 SC, Iowa City, IA 52242, USA

Received 1 July 2004; accepted 16 December 2004

Communicated by G.B. McFadden

Available online 26 January 2005

Abstract

An improved version of a previously developed mesoscopic model is used to simulate transients and thermal interactions during growth of equiaxed dendrites of a pure substance. The model is validated through comparisons with exact, analytical solutions and direct, fully resolved phase-field simulations. The issue of constancy in the selection parameter, σ^* , during transients is addressed in some detail. The model is first applied to realistically simulate previously performed microgravity experiments involving the growth of succinonitrile dendrites from a stinger inside a growth chamber. It is shown how the thermal interactions between the seed and the dendrite and between the growth chamber wall and the dendrite cause temporal variations in the dendrite tip velocities. Excellent agreement with microgravity measurements is obtained. A scaling relation is derived that provides the duration of the seed size effect during the initial transient. The model is also used to investigate the transients arising during the growth of two equiaxed dendrites towards each other. A scaling relation for the duration of the transient decay of the tip velocities is derived. Additional study is needed to fully understand cases where equiaxed grains interact early before a fully dendritic structure is established.

© 2005 Elsevier B.V. All rights reserved.

PACS: 68.70.+w; 81.30.Fb

Keywords: A1. Dendrites; A1. Growth models; B1. Succinonitrile

1. Introduction

Free growth of an isolated dendrite of a pure substance into a uniformly supercooled melt has been investigated extensively both as an example of a complex pattern formation process and due to applications in solidification of metals [1]. The issue of greatest fundamental interest is the

*Corresponding author. Tel.: +1 319 335 5681;
fax: +1 319 335 5669.

E-mail address: becker@engineering.uiowa.edu
(C. Beckermann).

relation between the steady-state dendrite tip velocity v , the radius of curvature of the tip R , and the far-field supercooling $\Delta T = T_m - T_\infty$, where T_m is the melting temperature and T_∞ is the melt temperature at infinity. This problem is characterized by the presence of widely disparate length scales: the thermal diffusion length given by $l_t = \alpha/v$, the tip radius R , and the capillary length $d_0 = \gamma T_m c_p / L^2$, where α is the thermal diffusivity, c_p is the specific heat, γ is the surface tension, and L is the latent heat. In present theories of free dendritic growth, the long-range heat diffusion on the scale of l_t , is usually modeled using the Ivantsov solution [2], which treats the dendrite tip as an isothermal paraboloid of revolution in a semi-infinite melt. This solution, $\Omega = Iv(Pe)$, provides a relation between the tip Péclet number, $Pe = vR/(2\alpha)$, and the dimensionless supercooling $\Omega = \Delta T/(L/c_p)$. The problem of the stability or operating state of the dendrite tip on the scale of R is treated by considering the temperature variation of the solid/liquid interface caused by curvature and anisotropic surface tension [3]. A stability constant or selection parameter is introduced that provides a relation between the tip radius and velocity as $\sigma^* = 2d_0\alpha/(vR^2)$. The selection parameter is generally thought to be independent of the supercooling.

The microgravity diffusion controlled dendrite growth data of Glicksman and co-workers [4,5] have been used to experimentally validate the above theory of free dendritic growth. However, it was soon realized that it is difficult to grow a dendrite in a truly isolated manner as required by the theory. The most obvious problem is that the melt cannot be infinite in extent as required by the Ivantsov solution. The thermal interactions between a dendrite and finite-sized growth chamber walls, which are especially important at low tip velocities when l_t is large, have been analyzed by Pines et al. [6] and Sekerka et al. [7]. Other effects that have been identified to cause deviations from the theory are thermal interactions between the dendrite and its initial seed [8], trailing side branches [9], and neighboring dendrites [10]. However, the analytical theories that have been developed to model these effects [6–10] still assume a constant dendrite tip velocity.

Thermal interactions between a dendrite and its surroundings can generally be expected to result in transient growth with a non-constant tip velocity, as shown experimentally by LaCombe et al. [11]. Transient dendritic growth has received little attention in the literature, even though it is an issue of great practical importance. In metal castings, many equiaxed dendrites nucleate and grow simultaneously in a supercooled melt. The thermal (or solutal in the case of alloys) interactions between the grains will almost always cause transient growth. The thermal fields from neighboring dendrites will overlap as the dendrites grow towards each other, and the tip velocities will decrease with time until the supercooling is completely dissipated and any tip growth stops. Further solidification then occurs through thickening of the dendrite arms. The dynamics of such equiaxed solidification are strongly dependent on the distance between the grains or, in other words, the local nuclei density. For large distances, the thermal fields do not significantly overlap until late in the solidification process and the dendrites can grow relatively undisturbed for at least some time. Then, large dendritic structures can be observed in a casting. For smaller distances, as in grain refined castings, the thermal interactions can be so strong from the beginning that the grains retain a globulitic shape and dendritic growth does not take place. An attempt has been made to model the interactions between dendrites in an average sense, by basing the supercooling that drives dendritic growth on the time-varying average temperature (or solute concentration) in the “extradendritic” liquid between the grains [12]. This and similar approaches in modeling of the interactions between dendrites have resulted in many interesting predictions of the grain structure in castings [12–14]. However, averaged models are not well validated and many open questions remain regarding transient growth of multiple dendrites, including the nature of the thermal field between the dendrites and the tip operating state selection for a non-constant tip velocity.

In this study, transient dendritic growth is investigated by addressing the effects of both, the initial seed size and the thermal interactions between two neighboring dendrites, as well as a

combination of the two. The study relies on a previously developed three-dimensional “mesoscopic” simulation model [15]. The use of this model is motivated by the fact that direct numerical simulations of dendritic growth, using for example the phase-field method [16], in three dimensions and for the low supercoolings and large domain sizes present in experiments will not be possible in the near future. The mesoscopic model combines a numerical calculation of the transient (macro-) temperature field around the dendrites with an analytical (micro-) model for the dendrite tip velocities [17]. The micro- and macro-temperature fields are matched at a so-called grain envelope, which is a smooth surface connecting the tips of all growing dendrite branches of an equiaxed grain. The mesoscopic model relies on the above mentioned separation of length scales by assuming that the dendrite tip operating state selection is unaffected by variations in the thermal far field; in fact, the selection parameter σ^* is assumed known and constant. The latter assumption is carefully examined in the present study using direct, three-dimensional phase-field simulations of dendritic growth transients. Furthermore, some limited validation is provided by comparing results for transient dendritic growth with available data from the microgravity experiments (IDGE) of Glicksman and co-workers [4,5].

The mesoscopic simulation model is explained in greater detail in Section 2, together with several improvements that have been made since its first implementation [15]. Numerical issues and validation are addressed in Section 3. Transient dendritic growth from a finite-sized seed is investigated in Section 4. Section 5 is devoted to transients arising during the simultaneous growth of two dendrites towards each other. The conclusions are summarized in Section 6.

2. The mesoscopic simulation model

The mesoscopic simulation model is described in Steinbach et al. [15] and the reader is referred to that publication for all details. Here, only the basic ideas and some improvements to the original model are outlined. Fig. 1 illustrates an equiaxed

dendrite growing into a supercooled melt. The mesoscopic model relies on the separation of the length scales associated with the tip radius, R , and the thermal diffusion length, $l_t = \alpha/v$. This separation is especially pronounced at low supercoolings (about 3 orders of magnitude), which is the regime of interest here.

As shown in Fig. 1, a grain envelope (e) is defined as a smooth surface connecting the tips of the ‘active’ or growing branches of a dendrite. The envelope motion and the temperature field around the grain envelope(s) are calculated by the model. The micro-temperature field on the scale of the tip radius and the macro-temperature field outside of the envelope are matched over a so-called stagnant film. This stagnant film is bounded by a confocal envelope (ce) located at a distance δ_f ahead of the dendrite envelope. The stagnant film thickness is of the order of $10R$, but the mesoscopic model results are ultimately independent of the exact value of δ_f .

An analytical expression is used to describe the micro-scale processes at each dendrite tip and to determine the envelope growth velocity. It is based on the stagnant-film modified Ivantsov solution given by [17]

$$\Delta T_f = T_m - T_{ce} = L/c_p Pe \exp(Pe) \{E_1(Pe) - E_1[Pe(1 + 2\delta_f/R)]\}, \quad (1)$$

where $Pe = vR/(2\alpha)$ as before, E_1 is the exponential integral function, ΔT_f is the supercooling

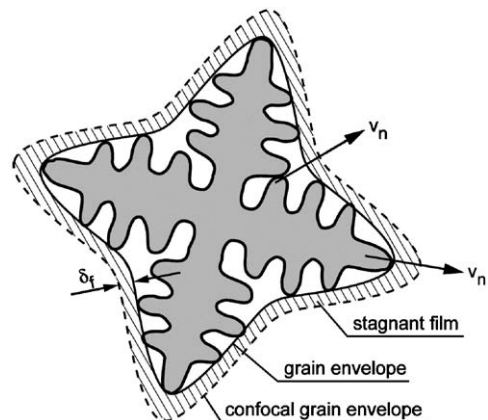


Fig. 1. Schematic illustration of the envelopes around an equiaxed dendrite as used in the mesoscopic model.

across the stagnant film, and T_{ce} is the temperature at a point on the confocal envelope. It can be seen that for $\delta_f/R \rightarrow \infty$, $T_{ce} \rightarrow T_\infty$ and Eq. (1) approaches the Ivantsov solution $\Omega = Iv(Pe)$. The above equation is coupled with the selection equation for R

$$R = \left(\frac{2d_0\alpha}{\sigma^*v} \right)^{1/2}. \quad (2)$$

Hence, the selection parameter σ^* is an input to the present model. Eqs. (1) and (2) are inverted numerically to obtain the dendrite tip velocity (or speed) v as a function of the confocal envelope temperature and the film thickness, i.e.,

$$v = f(T_{ce}, \delta_f). \quad (3)$$

The tip speed is converted to a normal envelope velocity v_n by

$$v_n = n v \cos \theta, \quad (4)$$

where n is the exterior normal vector to the envelope and θ is the angle between the normal and the growth axis of the nearest dendrite arm. This conversion is needed because the branches of a cubic dendrite do not always grow in a direction normal to the envelope (Fig. 1) [15]. It is important to realize that the envelope velocity varies from point to point on the envelope because the confocal envelope temperature, T_{ce} , is not constant (for a fixed film thickness δ_f). The confocal envelope temperature is obtained from the solution of the heat equation on a macroscopic scale, as explained next.

The temperature field in the melt around the grain envelope is obtained from a numerical solution of the following three-dimensional transient heat equation:

$$\frac{\partial T}{\partial t} = \alpha \nabla^2 T, \quad (5)$$

where t denotes times. At the boundary of the domain, as well as initially, the melt temperature is set to the value $T_\infty = T_m - \Delta T$ corresponding to the imposed supercooling. At each point on the grain envelope internal to the domain, the temperature is fixed to the effective envelope temperature T_e . The envelope temperature is initialized as T_m .

Critical to the coupling between the analytical micro-model and the macro-heat equation is the choice of the temperatures T_e and T_{ce} . Fig. 2 illustrates a small section of the stagnant film on the numerical grid used to solve the heat equation. The confocal envelope temperature, T_{ce} , is obtained from the numerical solution of the heat equation at the location of the confocal envelope. This can formally be written as

$$T_{ce} = T(x_{ce} = x_e + n\delta_f), \quad (6)$$

where x_e and x_{ce} are the position vectors of the grain envelope and the confocal envelope, respectively (Fig. 2). In the original model [15], the envelope temperature, T_e , was assumed to be equal to the melting temperature T_m , since the grain envelope touches the dendrite tips. Further numerical experimentation revealed that using $T_e = T_m$ leads to a somewhat inaccurate calculation of the temperature gradients in the stagnant film, because the microscopic temperature fields around each dendrite tip are not resolved in the numerical solution of the heat equation.

In order to obtain an improved estimate of the temperature T_e in the computational cells that contain the envelope, the following very approximate “sub-grid” model is employed. The envelope temperature T_e can be different from the melting temperature T_m because of steep microscopic temperature gradients around the dendrite tip on the scale of the numerical grid spacing Δx . In other

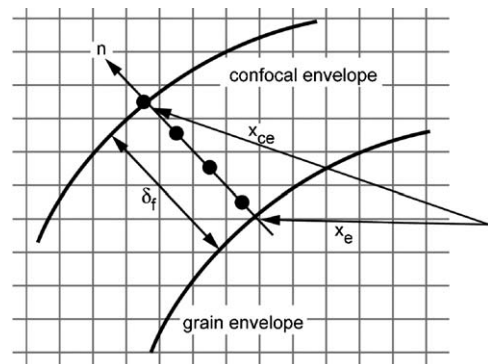


Fig. 2. Schematic illustration of the stagnant film on a numerical grid.

words, if the tip radius is small compared to the grid spacing, i.e. $R \ll \Delta x$, the temperature of the cell that contains the tip, T_e , should be lower than T_m . Only if the tip radius approaches or is larger than the grid spacing, i.e. $R \geq \Delta x$, can T_e be taken equal to T_m . A sub-grid stagnant film thickness, δ_{sg} , is introduced to measure the distance over which the temperature drop, $T_m - T_e$, occurs. For $R \ll \Delta x$, δ_{sg} is approximated as the half-diagonal of a cubic numerical cell, i.e., $\delta_{sg} \rightarrow \sqrt{3}/2\Delta x \approx 0.9\Delta x$. This half-diagonal can be interpreted as the distance corresponding to the maximum uncertainty in the position of the dendrite tip within a numerical cell. On the other hand for $R \geq \Delta x$, δ_{sg} should vanish. A relation that provides a smooth transition between these two limits can be written as

$$\delta_{sg}(R, \Delta x) = 0.9\Delta x \left(1 - \tanh \left(\frac{R}{0.9\Delta x} \right) \right). \quad (7)$$

The stagnant film model is now used to approximate the temperature drop, $T_m - T_e$, that occurs over the distance δ_{sg} , according to

$$T_e = T_m - f^{-1}(v, \delta_{sg}), \quad (8)$$

where f^{-1} is the inverse of the function given by Eq. (3). With Eq. (8), the temperature drop, $T_m - T_e$, increases with decreasing dendrite tip radius relative to Δx and increasing tip velocity. For $R \geq \Delta x$, Eq. (8) gives $T_e \rightarrow T_m$ regardless of the tip velocity and the original model of Ref. [15] is recovered. The above sub-grid model for calculating T_e is not intended to be physically rigorous. It should simply be viewed as a numerically justified method for approximating the microscopic temperature gradients around a dendrite tip within a numerical cell and, ultimately, for obtaining an improved estimate of the envelope temperature for the solution of the macro-heat equation.

From the above description of the present model it can be seen that there are two adjustable parameters: δ_f and Δx . They need to be chosen such that the solution of the model equations is independent of the stagnant film thickness δ_f and the grid size Δx , which is demonstrated in Section 3.

3. Numerical procedures and verification

The numerical solution procedure consists of a phase-field like propagation algorithm for the grain envelope and a control volume method for the heat equation, both of which are described in detail in Steinbach et al. [15]. The only modification implemented in this study is related to the phase-field like algorithm used to propagate the envelope on the numerical grid, which is briefly described next. A field variable ϕ is introduced that varies from 1 in the grain to 0 in the melt over a transition region of a thickness that, in the present study, is taken to be equal to the stagnant film thickness δ_f . This indicator function serves to track the propagation of the grain envelope and the confocal envelope, which are assigned values of $\phi = 0.95$ and 0.05 , respectively. The equation that propagates ϕ with the normal envelope velocity \mathbf{v}_n is given by

$$\frac{\partial \phi}{\partial t} = \frac{6}{\delta_f} \phi(1 - \phi)|\mathbf{v}_n| + \text{stab}(\phi). \quad (9)$$

All grid points in the normal direction across the transition region (Fig. 2) are assigned the same $|\mathbf{v}_n|$. The stabilization operator $\text{stab}(\phi)$ acts as an anti-diffusion flux that keeps the ϕ profile compact. The new expression developed for the stabilization operator in this study is given by

$$\text{stab}(\phi) = C \left[\frac{\delta_f^2}{72} \nabla^2 \phi - \phi(1 - \phi)(0.5 - \phi) - \left\langle \frac{\delta_f^2}{72} \nabla^2 \phi - \phi(1 - \phi)(0.5 - \phi) \right\rangle_n \right], \quad (10)$$

where $C \approx 0.1/\Delta t$ is a stabilization constant, Δt is the time increment, and $\langle \cdot \rangle_n$ denotes an average over the film thickness δ_f in the normal direction. Note that $\langle \text{stab}(\phi) \rangle_n = 0$, implying that the stabilization does not introduce a net driving force for the envelope motion. The new stabilization operator given by Eq. (10) proved to be easier to implement and provided more reliable results than the original version in Ref. [15].

Example model predictions for dendritic growth of a single equiaxed grain into a uniformly supercooled melt are shown in Fig. 3. Properties

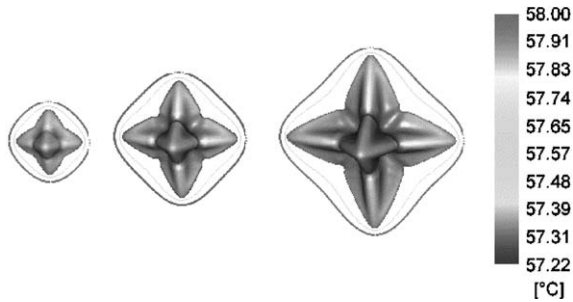


Fig. 3. Example model predictions of the evolution of the confocal envelope for a single equiaxed dendrite; the gray shades indicate the confocal envelope temperature and, indirectly, the growth velocity on each point of the envelope.

used are those of succinonitrile (SCN) and $\sigma^* = 0.02$ [5,18]. The surface in Fig. 3 represents the confocal envelope, with the gray shades indicating the temperature on the envelope, T_{ce} . A few isotherms in the surrounding melt are also shown. It can be seen that a realistic envelope shape, typical of a cubic dendrite, is predicted. The variations in the confocal envelope temperature reflect the different envelope growth velocities according to Eq. (3).

3.1. Steady-state growth

The model was first validated for a single equiaxed grain growing into an infinite melt by comparing predictions for the steady-state dendrite tip velocity to the analytical value from the Ivantsov solution coupled with the selection equation for R . For this purpose, the domain size was chosen large enough that the thermal field does not interfere with the boundary. Fig. 4 shows the percent difference between the tip velocity predicted by the present model and the one from the Ivantsov solution, denoted by v_{iv} , as a function of the film thickness δ_f and various grid spacings Δx . The results are for a representative supercooling of 0.65 K and SCN properties. It was found that in all cases a ratio of $\delta_f/\Delta x \approx 5 - 7$ works best, as already anticipated. It can be seen that for relatively fine grids of $\Delta x \leq 200 \mu\text{m}$, the error is less than about 2%, which is better than for the original model [15]. For $\Delta x = 400 \mu\text{m}$, the error increases to about 5%, which can be

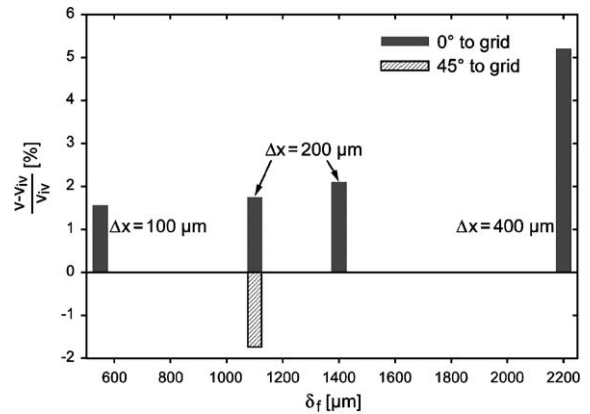


Fig. 4. Percent error of the dendrite tip velocity predicted by the mesoscopic model relative to the analytical solution for a free dendrite; the error is shown as a function of the stagnation film thickness, the grid spacing, and the orientation of the dendrite with respect to the numerical grid.

attributed to δ_f approaching the thermal diffusion length l_t . The two results in Fig. 4 for $\Delta x = 200 \mu\text{m}$ indicate that the error is relatively independent of δ_f . Finally, the two results in Fig. 4 (with $\Delta x = 200 \mu\text{m}$) for the dendrite growing aligned with the grid (0°) and diagonal to the grid (45°) indicate that there is a small grid anisotropy effect of about $\pm 2\%$ that can be tolerated. It should be noted that additional aspects of steady-state model predictions were verified against microgravity experimental data [19] in Ref. [15]. Good agreement was obtained for the envelope shape and the average internal solid fraction variation.

3.2. Transient growth

Validation of the present mesoscopic simulation model in the transient regime is difficult, because no analytical solution or well-defined experimental results for transient dendritic growth exist. Therefore, transient predictions of the present model are compared to corresponding results from direct, fully resolved simulations of dendritic growth using the three-dimensional phase-field model of Karma et al. [20]. The conditions for such a comparison need to be chosen such that both models yield accurate results in a reasonable computational time. For that reason, the

phase-field calculations are performed using an artificially large surface tension anisotropy of 2.5%, rather than the 0.5% that is typical of SCN. All other properties are chosen to be those of SCN. For a supercooling of 0.578 K and the 2.5% surface tension anisotropy, the phase-field model gives a steady-state value of the selection parameter of $\sigma^* = 0.065$. The selection parameter is obtained by measuring the steady-state dendrite tip radius and velocity from the simulation results and substituting them into Eq. (2) after solving it for σ^* . The 0.065 value is then used in all mesoscopic model simulations in this section. The difference between $\sigma^* = 0.065$ and the value of 0.02 typically used for SCN at low supercoolings [5,18] can be explained by the well-known dependence of σ^* on the surface tension anisotropy [20]. Again, the artificial increase of the surface tension anisotropy by about a factor of five over the value for SCN is done in the phase-field simulations of this subsection only to facilitate a direct comparison between the phase-field and mesoscopic simulations. The mesoscopic simulations in the following sections use again a value for σ^* that corresponds to the actual surface tension anisotropy of SCN.

First, the predictions of the mesoscopic model are compared to the phase-field results for growth from a spherical seed into an essentially infinite supercooled melt. As in Section 3.1, the domain size for the simulations was chosen large enough that the thermal field does not interfere with the boundary. The initial temperature of the melt in both the mesoscopic and the phase-field simulations is set uniformly to $T_\infty = T_m - 0.587$ K. The initial temperature of the seed in the phase-field simulations is also taken to be T_∞ , whereas the initial envelope temperature in the mesoscopic simulations is T_m , as before. Fig. 5 shows calculated dendrite tip velocities as a function of time up to 1.5 s, which is close to reaching a steady growth state. The horizontal dashed line indicates the steady tip velocity obtained analytically using the Ivantsov solution together with the selection equation, Eq. (2). The two mesoscopic model results included in Fig. 5 are for two different initial seed sizes and also correspond to two different grid spacings (10 and 20 μm). It can be

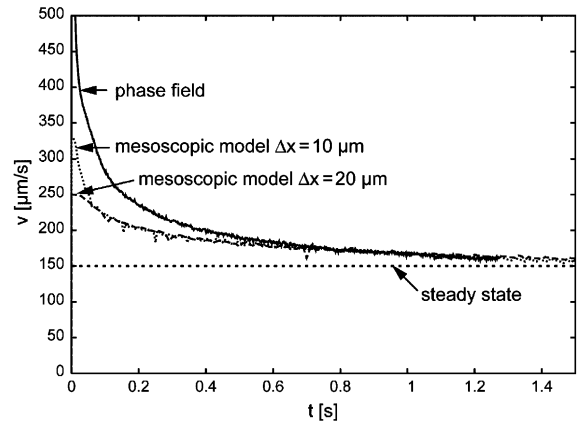


Fig. 5. Comparison of the variation of the dendrite tip velocities predicted by the mesoscopic model and the phase-field model for a single dendrite growing from a seed into an infinite supercooled melt (parameters provided in text); mesoscopic model results are shown for two different seed sizes; the seed size in the phase-field simulation is one order of magnitude smaller than in the mesoscopic model simulations.

seen that the tip velocities from the two mesoscopic simulations converge to the same values after a short initial transient that is caused by the different seed sizes. Both mesoscopic model results approach the phase-field predictions after an initial transient of about 0.6 s. The differences before that time are primarily due to the fact that a much smaller (about a factor of ten in diameter) seed was used in the phase-field simulation (which uses a grid spacing of 0.366 μm). The small seed in the phase-field simulation causes much higher initial growth velocities. Some differences are also due to the fact that the mesoscopic model assumes a constant σ^* during the very first growth stages from a spherical seed, which is known from the phase-field simulation to be not the case. Nonetheless, the good agreement during the later stages of growth establishes some confidence in being able to compare mesoscopic and phase-field simulations during slow transients, using a σ^* from steady-state phase-field results in the mesoscopic model. This is remarkable because the grid spacing in the mesoscopic simulations is up to 50 times larger than in the phase-field simulations.

In order to investigate in more detail the performance of the mesoscopic model for rapid

growth transients, it is compared to phase-field predictions using the following numerical test. Growth transients are artificially introduced in the simulations by suddenly changing the melting temperature, T_m , to a different value, while leaving the far-field temperature, T_∞ , at the same value. Such a jump in the melting temperature could be achieved in practice by exploiting the pressure dependence of the melting point (Clausius–Clapeyron effect). Two different test cases are considered: (Case 1) the simulations are started with a T_m that is 0.23 K *higher* than the actual value for SCN and continued until the dendrite tip velocities predicted by the mesoscopic and phase-field models agree, and then (at approximately 0.45 s) T_m is instantaneously *decreased* to the actual value for SCN; (Case 2) the simulations are started with a T_m that is 0.23 K *lower*, and then (at approximately 1.0 s) T_m is *increased* to the actual value for SCN. Other conditions are the same as for the phase-field simulation of Fig. 5.

The results in Fig. 6 indicate that in both cases, the dendrite tip velocity changes almost instantaneously in response to the change in the melting temperature. The direct simulation with the phase-field model predicts in Case 1 (2) a sudden decrease (increase) in the tip velocity to a value much below (above) the final steady-state tip velocity, a rapid increase to a value slightly above (below) the final steady-state tip velocity, followed by a more gradual transient during which the tip velocity approaches the final steady-state value. The tip velocities predicted by the mesoscopic model generally agree with the phase-field results. However, the initial “overshoot” in the tip velocity is not as pronounced in the mesoscopic model results and, consequently, some deviations between the results of the two models exist in the ensuing gradual approach to the steady state. It can be expected that these differences are due to the assumption of a constant σ^* in the mesoscopic model. No such assumption is needed in the phase-field model.

Fig. 7 shows the variation of the selection parameter, σ^* , predicted by the phase-field model for both cases. It can be seen that σ^* is approximately constant except for a pronounced spike immediately following the change in the

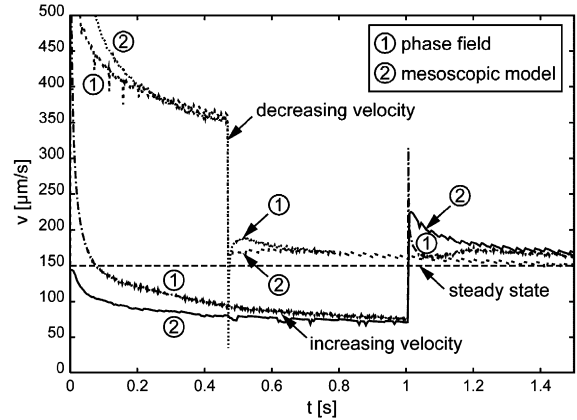


Fig. 6. Comparison of the variation of the dendrite tip velocities predicted by the mesoscopic and the phase-field model for a single dendrite growing from a seed into an infinite supercooled melt with a step change in the melting temperature (parameters provided in text); results are shown for two cases: a decrease in the melting temperature at 0.45 s leading to a decreased tip velocity, and an increase in the melting temperature at 1.0 s leading to an increased tip velocity.

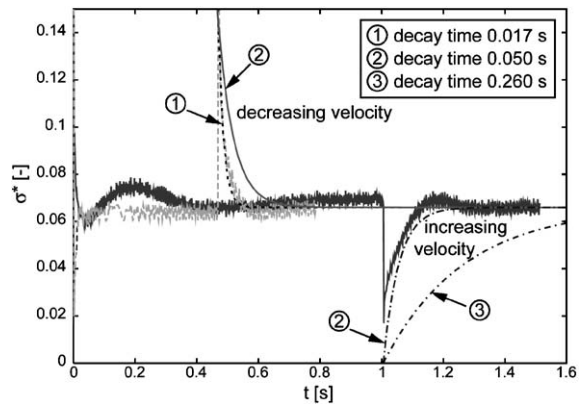


Fig. 7. Variation of the selection parameter, σ^* , predicted by the phase-field model for the same two simulation cases as in Fig. 6; the dashed lines are fits of the decays in σ^* given by Eq. (12) and different decay times.

melting temperature. It is important to note that σ^* is constant during the slow approach to steady state, before the change in the melting temperature, even though the tip velocities are still changing considerably (see Fig. 6). This indicates that the assumption of a constant σ^* in the mesoscopic model is reasonable for relatively slow

growth transients. Focusing now on the spike following the change in T_m , it can be seen that in Case 1 (2), σ^* first increases (decreases) abruptly to a value that is more than twice (less than half) the steady-state value, and then decays (increases) more gradually back to the steady-state value of $\sigma^* = 0.065$. The duration of the spike in σ^* in Case 1 (2) is about 0.02 s (0.05 s). The spike in σ^* can be expected because the tip velocity changes abruptly in response to the change in T_m (see Fig. 6), whereas the dendrite tip radius needs some time to adjust because growth (or melting) is needed for the dendrite to change its shape. After the spike, the selection parameter σ^* returns to the same value as before the change in T_m , confirming that σ^* is indeed independent of the supercooling.

In order to obtain a better understanding of the conditions under which the mesoscopic model becomes inaccurate, it is useful to provide an approximate analytical expression for the characteristic decay time, t_d , during which σ^* cannot be expected to be constant. It is assumed that in order for the dendrite tip to adjust its shape after a sudden change in the supercooling (until σ^* becomes constant again), it needs to grow by a distance equal to half its tip radius. Hence, an order of magnitude estimate of the characteristic decay time, t_d , is given by

$$t_d = \frac{R}{2v}. \quad (11)$$

The estimate given by Eq. (11) is tested by comparing it to the phase-field predictions in Fig. 7 for both simulation cases. The predicted decay in σ^* is assumed to be described by the following exponential

$$\sigma^* = \Delta\sigma \exp\left(-\frac{t-t_0}{t_d}\right), \quad (12)$$

where t_0 is the time when the change in T_m occurs. The amplitude $\Delta\sigma$ of the change in σ^* at $t = t_0$ can be estimated by assuming that the tip velocity changes instantaneously, while the tip radius keeps its value from before the change in T_m . Using Eq. (2), the amplitude $\Delta\sigma$ is then given by

$$\Delta\sigma = \frac{2d_0\alpha}{(R_1)^2} \left(\frac{1}{v_1} - \frac{1}{v_2}\right), \quad (13)$$

where the subscripts 1 and 2 indicate the states before and after the spike in σ^* , respectively. The tip radii and velocities at states 1 and 2 are readily obtained from the phase-field simulation results. The decay time, t_d , in Eq. (12) is calculated from the estimate given by Eq. (11). Curves for the σ^* variation given by Eq. (12) are included in Fig. 7 for the following values of the decay time t_d : Case 1: $R_1/(2v_1) = 0.017$ s and $R_2/(2v_2) = 0.05$ s; Case 2: $R_1/(2v_1) = 0.26$ s and $R_2/(2v_2) = 0.05$ s. It can be seen that in each case, the shorter decay time ($R_1/(2v_1)$ in Case 1 and $R_2/(2v_2)$ in Case 2) results in an excellent fit with the σ^* variation predicted by the phase-field model. While it is not immediately clear why the shorter decay times result in a better fit with the phase-field predictions in both cases, it is apparent that the simple estimate of the decay time given by Eq. (11) provides the correct order of magnitude of the time during which σ^* is not constant after a sudden change in the melting temperature.

In conclusion, the above comparisons with the phase-field model show that the mesoscopic model generally provides good results during transient dendritic growth. As expected, inaccuracies arise during rapid transients when the selection parameter σ^* is not constant. Variations in σ^* are limited to relatively small time scales of the order of $t_d = R/(2v)$.

4. Transient growth of a single dendrite from a finite-sized seed inside a growth chamber

The mesoscopic model is now used to simulate the microgravity experiments (IDGE) of Glicksman and co-workers [4,5] involving the growth of SCN dendrites from a stinger inside a uniformly supercooled melt volume that is contained by a growth chamber. As discussed in the Introduction, the main issues to be investigated are the effects of the thermal interactions between the dendrite and its initial seed and also between the dendrite and the chamber walls. These interactions can result in a non-constant dendrite tip velocity.

Three representative experiments with imposed supercoolings of 0.37, 0.78, and 1.01 K are simulated using the mesoscopic model, and the

predicted dendrite tip velocities are compared to experimental data. The tip velocities were measured by analyzing microgravity experiment images that were supplied to the authors directly by NASA. Some of the measurement procedures, including the corrections made to account for the orientation of the dendrite with respect to the cameras, are explained in Refs. [18,19]. The measured tip velocities are plotted as symbols in Figs. 8a–c for each of the three supercoolings. Error bars that represent the estimated uncertainty in the velocity measurements are included in the figures. The time scale does not start at the initiation of growth ($t = 0$) because no measurements were possible at early times. In Fig. 8c, data are included from two arms of the same dendrite, and it can be seen that they coincide with each other to within the experimental uncertainty. For the lowest supercooling (0.37 K, Fig. 8a) the measured tip velocities are approximately constant in time. A significant rise in the tip velocities is observed in the experiments with the 0.78 and 1.01 K supercoolings (Figs. 8b and c). These observations are explained in detail below when the measurements are compared to the predictions.

In the mesoscopic model simulations the growth chamber is approximated as a sphere with a radius of 16 mm. The walls of the growth chamber, as well as initially the melt, are taken to be isothermal at a temperature corresponding to the imposed supercooling. A finite-sized seed is placed at the center of the domain. In the microgravity experiments, growth is initiated from a capillary tube (or stinger) with an inner radius of 1.2 mm. However, during initiation, the solid SCN propagates mostly in a thin layer along the inside of the tube rather than filling the entire tube. Furthermore, the solid forms an uneven “ring” around the end of the tube before a single dendrite emerges from the small instabilities on the ring. Therefore, it is difficult to establish an accurate effective seed size for use in the simulations and each experiment is simulated twice using two different seed sizes. A large seed of approximately $900\ \mu\text{m}$ radius is used in one set of simulations. This seed size is intended to be representative of the actual experimental conditions and results in good agreement of the predicted tip velocities with the experimental data

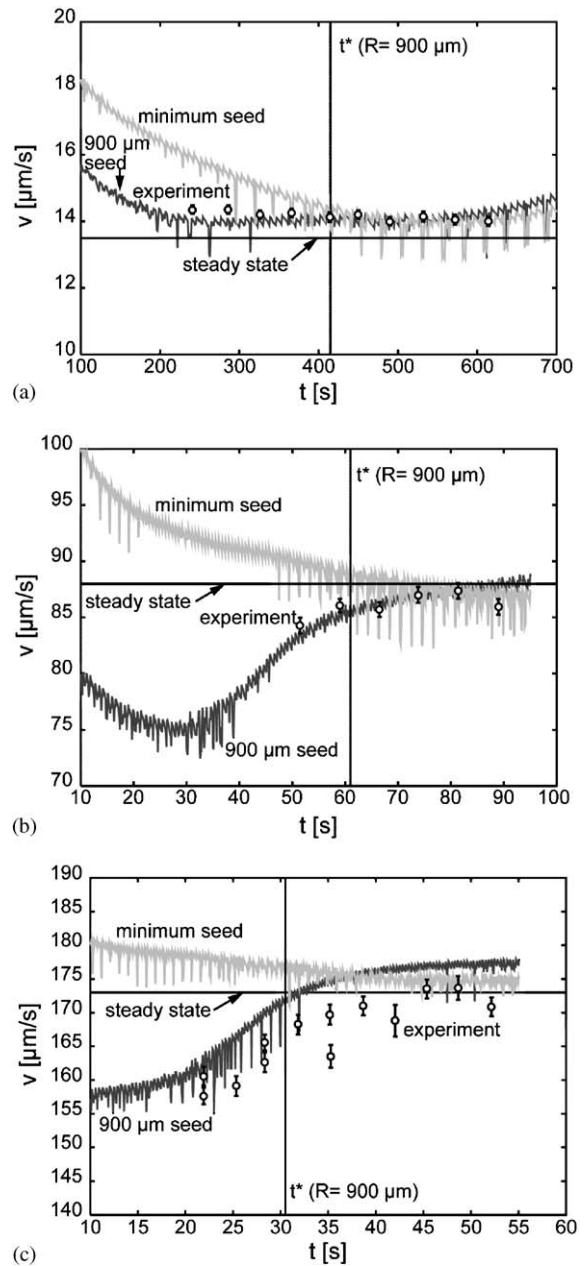


Fig. 8. Variation of the dendrite tip velocities predicted by the mesoscopic model for a SCN dendrite growing from two different size seeds (“minimum” and $900\ \mu\text{m}$ radius) inside a growth chamber and comparison to IDGE data for three different supercoolings: (a) 0.37 K, (b) 0.78 K, and (c) 1.01 K; the vertical line indicates the characteristic time given by Eq. (14) for the $900\ \mu\text{m}$ seed radius.

for all three supercoolings (see below). The second set of simulations is performed with a “minimal” seed that corresponds to the size, Δx , of one (cubic) computational cell. The edge lengths of the computational cells are taken as $\Delta x = 200 \mu\text{m}$ for the 0.37 K supercooling and $\Delta x = 100 \mu\text{m}$ for the 0.78 and 1.01 K supercoolings. A selection parameter equal to $\sigma^* = 0.018$ is used in all simulations; this value provides slightly better agreement with the microgravity experimental data at steady state than the 0.02 value used earlier.

Figs. 8a–c show the calculated time evolutions of the tip velocity for each of the three supercoolings. The horizontal solid line in each plot indicates the steady-state value of the tip velocity, v_{iv} , obtained analytically from the Ivantsov solution together with $\sigma^* = 0.018$. It is obvious that the initial seed size has a dramatic effect on the tip velocity before a steady state is reached. For the “minimal” seed, the tip velocities decrease monotonically until they reach a constant value that is close to v_{iv} . On the other hand, for the $900 \mu\text{m}$ seed the tip velocities first reach a minimum that is much below the steady-state value (except for the lowest supercooling) and then increase to approach the steady-state value. This increase in the tip velocities is in good agreement with the experimental data for the two higher supercoolings (Figs. 8b and c). Although the measured tip velocities for the lowest supercooling are approximately constant (Fig. 8a), the predictions for the $900 \mu\text{m}$ seed are clearly in much better agreement with the experimental data than the ones for the “minimal” seed.

The observed thermal interactions between the dendrite and its seed can be explained by the presence of a spherical heat diffusion field that emanates from the seed. During early times the dendrite grows inside this spherical diffusion field. This results in lower tip velocities because the temperatures are locally higher. At later times, the dendrite tips escape the spherical diffusion field, the temperatures around the tips approach those given by the Ivantsov solution, and the tip velocities increase toward the steady-state value. From the solution of the steady heat equation for diffusion from a sphere, the thickness of the thermal boundary layer around the initial spher-

ical seed can be estimated to be equal to $6R_s$, where R_s is the seed radius. Hence, the time, t^* , for a dendrite tip (growing at a velocity v_{iv}) to traverse the spherical diffusion field from the seed is given by

$$t^* = \frac{6R_s}{v_{iv}}. \quad (14)$$

This characteristic time, with $R_s = 900 \mu\text{m}$, is indicated as a vertical line in Figs. 8a–c. For the “minimal” seed, t^* is so small that the effect of the initial seed size can be neglected. It can be seen that the predicted tip velocities for the minimal seed and the $900 \mu\text{m}$ seed merge into a single curve at the characteristic time t^* ($R_s = 900 \mu\text{m}$) for all three supercoolings. This indicates that Eq. (14) indeed provides an excellent estimate of the time during which the initial seed has a significant effect on the tip velocities.

For the lowest supercooling (0.37 K, Fig. 8a) the mesoscopic model predictions as well as the measured tip velocities do not show a minimum. In fact, the tip velocities remain slightly above the steady-state value given by the Ivantsov solution together with $\sigma^* = 0.018$. Furthermore, the mesoscopic model predicts a slight increase in the tip velocity towards the end of the simulation (between 600 and 700 s). These observations can be explained by the thermal interactions between the dendrite and the growth chamber wall. Such interactions tend to increase the tip velocity because the thermal gradients become steeper as the dendrite tip approaches the isothermally held wall. For the 0.37 K supercooling the thermal diffusion length ahead of the dendrite tip, $l_t = \alpha/v_{iv}$, is approximately equal to 8.5 mm, which is not small relative to the radius of the growth chamber (16 mm). Hence, the dendrite can be expected to begin to “feel” the effect of the chamber wall almost from the beginning of growth ($t \geq 200$ s). The combination of the effects of the initial seed, which reduce the tip velocity for $t < t^* = 400$ s, and of the chamber wall, which tend to increase the tip velocity, then result in an almost constant tip velocity, slightly above the Ivantsov value, between 200 and 400 s for the 0.37 K supercooling. The increase in the tip velocity beyond 600 s is solely due to the effect of the

proximity of the chamber wall. For the 0.78 and 1.01 K supercoolings, the thermal diffusion lengths ahead of the dendrite tips are only about 1.3 and 0.7 mm, respectively. These lengths are small enough relative to the size of the growth chamber that the thermal interactions between the dendrite and the chamber wall are negligible during the growth period analyzed and the dendrite can reach a steady growth state. It should be mentioned that in Fig. 8c the small deviations (less than 3%) of the predicted steady-state tip velocities from the Ivantsov value are within the accuracy of the mesoscopic model calculations (see Section 3.1).

5. Analysis of the transient growth of impinging dendrites

Additional mesoscopic model simulations are performed to investigate the transients arising during the simultaneous growth of two dendrite arms directly towards each other. Fig. 9 shows the results of an example calculation for an imposed supercooling of 0.58 K and a seed distance, D_{seed} , of 1 cm. It can be seen that the temperature profiles ahead of the dendrite tips are starting to overlap at approximately 10 s. After that time, the temperature at the center between the two tips starts to increase and the tip velocities decrease. At 90 s, the supercooling between the dendrites is almost

completely dissipated and the tip velocities approach zero. Using the results from Section 3.2, it can be shown that the transients in the present simulations of the growth of impinging dendrites are generally slow enough that σ^* can indeed be assumed constant.

Fig. 10 shows predicted variations in the tip velocities for simulations with a relatively large seed distance, D_{seed} , of 10 cm (and a seed size of 300 μm) and five different supercoolings ranging from 0.2 to 0.65 K. The results for all supercoolings are presented in a single plot, using linear (instead of logarithmic) scales, in order to more clearly demonstrate the large range of tip velocities predicted and the fact that the times when the tip velocities approach zero range from tens of seconds to several hours. It can be seen that after a short initial transient, the tip velocities generally reach a plateau, which is indicative of a steady state. Then, they decay to zero in a transient that is due to thermal interactions between the dendrites.

The decays of the tip velocities in Fig. 10 for the different supercoolings can be scaled by non-dimensionalizing the tip velocities with v_{iv} , and time with a characteristic transient time, t_t . This characteristic decay time is given by the ratio of the thermal diffusion length, $l_t = \alpha/v_{iv}$, to v_{iv} as

$$t_t = \frac{l_t}{v_{iv}} = \frac{\alpha}{v_{iv}^2}. \tag{15}$$

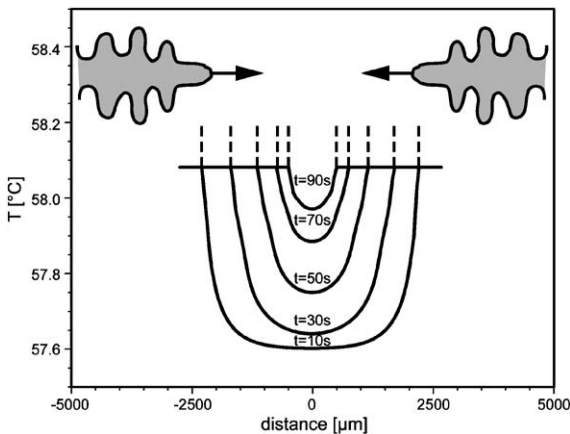


Fig. 9. Predicted variation of the temperature profile between two equiaxed dendrites growing towards each other (parameters provided in text).

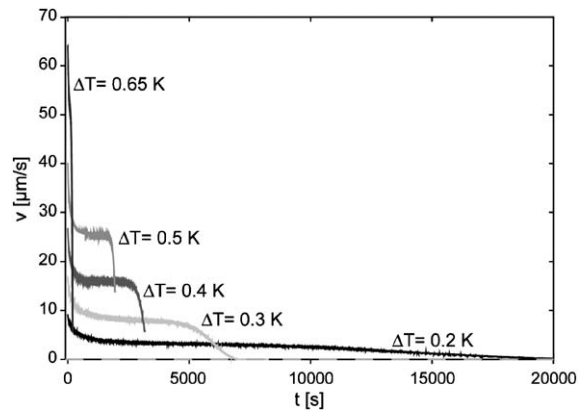


Fig. 10. Predicted variation of the dendrite tip velocity for two equiaxed dendrites growing towards each other for five different supercoolings (parameters provided in text).

The decay of the tip velocities due to thermal interactions between the dendrites occurs at different times during a simulation depending on the initial seed distance. Hence, in scaling the decays, the time in each simulation needs to be shifted by an amount equal to the so-called interaction time, t_i . The interaction time is defined here as the time when the tip velocity has decreased to $0.5v_{iv}$. Then, the final definition of the scaled time is given by

$$\tau = \frac{t - t_i}{t_t} \quad (16)$$

Fig. 11 shows the scaled tip velocities, v/v_{iv} , as a function of the scaled time, τ . In addition to the results from Fig. 10, predictions from simulations for supercoolings of 0.8 and 1.0 K are also included. It can be seen that the scaled tip velocities show approximately the same decay for all supercoolings. This indicates that the above scaling of the transients due to thermal interactions between the dendrites is essentially correct.

In order to quantitatively measure the actual duration of the decay in the tip velocities, the following hyperbolic tangent profile can be fit to the results in Fig. 11

$$\frac{v}{v_{iv}} = 0.5 \left(1 - \tanh \frac{\tau}{\tau_t} \right), \quad (17)$$

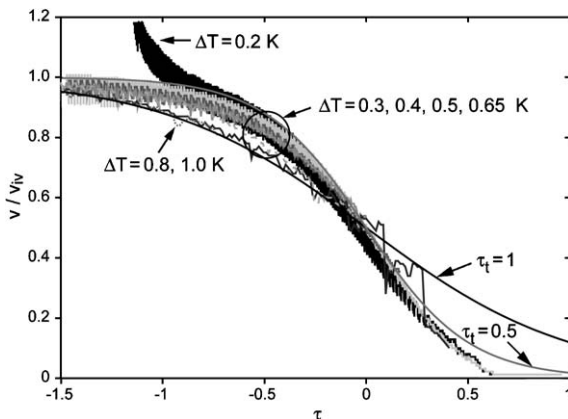


Fig. 11. Scaled decays in the dendrite tip velocity for two equiaxed dendrites growing towards each other for seven different supercoolings (same cases as in Fig. 10 plus two additional supercoolings); fits given by Eq. (17) are included for two different dimensionless decay times (0.5 and 1).

where τ_t is a measure of the duration of the decay. Profiles for $\tau_t = 1$ and 0.5 are included in Fig. 11. It can be seen that the profile with $\tau_t = 0.5$ provides a relatively good fit of the decays in the tip velocities predicted by the mesoscopic model for all supercoolings. The profile with $\tau_t = 1$ gives a somewhat better fit during the initial part of the decay for the two highest supercoolings (0.8 and 1.0 K). Note that $\tau_t = 0.5$ implies that the duration of the decay in the tip velocities is equal to $0.5l_t/v_{iv}$. These results show that, as expected, significant thermal interactions between two dendrites start to take place when the tips are within about one (for $\tau_t = 0.5$) to two (for $\tau_t = 1$) thermal diffusion lengths, l_t , of each other.

The simulations in Figs. 10 and 11 are for a seed distance, D_{seed} , large enough (10 cm) that, for all supercoolings, the dendrites can reach a steady growth stage before interacting with one another. The effect of the initial seed distance is investigated next by performing simulations for a supercooling of 0.65 K and seed distances of 14, 20, and 26 mm. The results in Fig. 12 show that for the two smaller seed distances the dendrite tip velocity does not attain the steady-state value ($\approx 58 \mu\text{m/s}$) before the onset of the decay due to thermal interactions between the dendrites. In fact, for the 14 mm seed distance, the initial transient due to growth from a seed and the decay due to thermal interactions

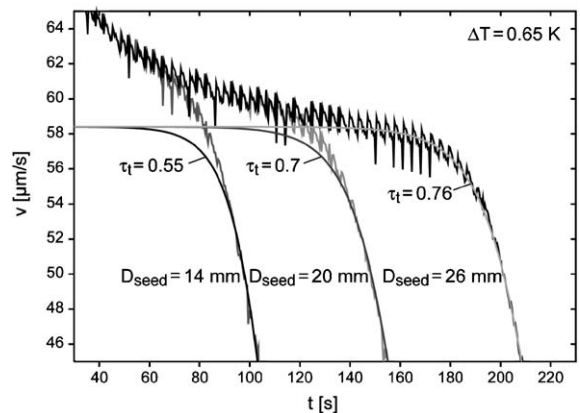


Fig. 12. Predicted variations of the dendrite tip velocity for two equiaxed dendrites growing towards each other for three different seed distances (parameters provided in text); fits given by Eq. (17) are included for each seed distance.

overlap so strongly that the tip velocity decreases steeply throughout the simulation. Furthermore, from the fit of the decays in Fig. 12 by the hyperbolic tangent profile, Eq. (17), it can be seen that the characteristic decay time τ_t decreases from 0.76 to 0.55 for the seed distance decreasing from 26 to 14 mm. This indicates that, as expected, the decay time is reduced if the dendrites start to thermally interact early before they reach a steady growth state. A detailed analysis of the transient evolution of the tip velocities for even smaller seed distances is beyond the scope of the present study. For such small seed distances, there is insufficient time for a regular dendrite morphology to develop (i.e., the grains will retain a globulitic shape) and the present mesoscopic model cannot be expected to be applicable.

6. Conclusions

An improved version of a previously developed mesoscopic dendrite simulation model is used to investigate transients and thermal interactions arising during equiaxed growth. The model is validated (i) for steady-state growth against the standard analytical model for free dendritic growth and (ii) for transient growth against direct, fully resolved phase field simulations. It is found that in the presence of transients inaccuracies in the mesoscopic model predictions are limited to a short response time during which the selection parameter, σ^* , is not constant. The transient response time due to a sudden change in the melting temperature is of the order of $R/2v$.

The model is first applied to realistically simulate the IDGE of Glicksman and coworkers [4,5]. Both the seeding procedure and the growth chamber walls are modeled in the simulations. Excellent agreement with the measured variations in the dendrite tip velocities is obtained for a range of imposed supercoolings. It is shown that the size of the initial seed size has a profound influence on the initial transient during which the tip velocity approaches the steady state. The thermal field from a relatively large seed tends to reduce the tip velocity (below the steady-state value) during the initial transient, which is supported by the experi-

mental data. A scaling relation is derived for the duration of the initial seed size effect. It is also found that for a relatively low supercooling, the thermal interactions with the growth chamber walls, which tend to increase the tip velocity, are important almost from the beginning of growth. The combination of the seed and wall effects results in an almost constant tip velocity during much of the duration of the experiment with a low supercooling.

The mesoscopic model is then used to investigate the transients arising due to thermal interactions during the growth of two equiaxed dendrites towards each other. The results show how the supercooling between the dendrites is dissipated and the tip velocities decrease. A scaling relation for the transient decay of the tip velocities is derived. Some results are also presented for the case where the initial transient due to growth from a seed and the decay due to thermal interactions between dendrites overlap. However, additional study is needed to quantify the evolution of the growth velocities in such cases.

Acknowledgments

This work was supported, in part, by DARA under contract 50WM0035 and by NASA under contracts NCC8-094 and NNM04AA18G. The authors thank Dr. Qiao Li, formerly of The University of Iowa, for his help with the dendrite tip velocity measurements. We also thank Dr. Matthis Plap of the Ecole Polytechnique, Paris, and Dr. Alain Karma of Northeastern University, Boston, for providing the 3-D phase-field code.

References

- [1] M.E. Glicksman, S.P. Marsh, in: D.J.T. Hurle (Ed.), Handbook of Crystal Growth, vol. 1, Part b, Elsevier, Amsterdam, 1993, p. 1077.
- [2] G.P. Ivantsov, Dokl. Akad. Nauk SSSR 58 (1947) 56.
- [3] J.S. Langer, Science 243 (1989) 1150.
- [4] M.E. Glicksman, M.B. Koss, E.A. Winsa, Phys. Rev. Lett. 73 (1994) 573.

- [5] M.B. Koss, J.C. LaCombe, L.A. Tennenhouse, M.E. Glicksman, E.A. Winsa, *Metall. Mater. Trans. A* 30A (1999) 3177.
- [6] V. Pines, A. Chait, M. Zlatkowski, *J. Crystal Growth* 167 (1996) 383.
- [7] R.F. Sekerka, S.R. Coriell, G.B. McFadden, *J. Crystal Growth* 171 (1997) 303.
- [8] V. Pines, A. Chait, M. Zlatkowski, *J. Crystal Growth* 182 (1997) 219.
- [9] J.C. LaCombe, M.B. Koss, D.C. Corrigan, A.O. Lupulescu, J.E. Frei, M.E. Glicksman, *J. Crystal Growth* 206 (1999) 331.
- [10] V. Pines, A. Chait, M. Zlatkowski, C. Beckermann, *J. Crystal Growth* 197 (1999) 355.
- [11] J.C. LaCombe, M.B. Koss, M.E. Glicksman, *Phys. Rev. Lett.* 83 (1999) 2997.
- [12] C.Y. Wang, C. Beckermann, *Metall. Mater. Trans. A* 27A (1996) 2754.
- [13] Ch.A. Gandin, M. Rappaz, *Acta Metall.* 42 (1994) 2233.
- [14] M.A. Martorano, C. Beckermann, Ch.A. Gandin, *Metall. Mater. Trans. A* 34A (2003) 1657.
- [15] I. Steinbach, C. Beckermann, B. Kauerauf, Q. Li, J. Guo, *Acta Mater.* 47 (1999) 971.
- [16] W.J. Boettinger, J.A. Warren, C. Beckermann, A. Karma, *Ann. Rev. Mater. Res.* 32 (2002) 163.
- [17] B. Cantor, A. Vogel, *J. Crystal Growth* 14 (1977) 109.
- [18] Q. Li, C. Beckermann, *J. Crystal Growth* 236 (2002) 482.
- [19] Q. Li, C. Beckermann, *Phys. Rev. E* 57 (1998) 56.
- [20] A. Karma, Y.H. Lee, M. Plapp, *Phys. Rev. E* 61 (2000) 3996.